

UAV-assisted underlay CR-NOMA network: performance analysis

Dinh-Thuan Do, Chi-Bao Le

Faculty of Electronics Technology, Industrial University of Ho Chi Minh City, Ho Chi Minh City, Vietnam

Article Info

Article history:

Received Jun 7, 2021

Revised Apr 24, 2022

Accepted May 31, 2022

Keywords:

Imperfect SIC

Interference management

Nakagami- m fading

NOMA

UAV

ABSTRACT

We highlight the potential of non-orthogonal multiple access (NOMA) integration with unmanned aerial vehicle (UAV) for future communications networks in beyond 5 generation (B5G) networks to enhance cellular communication, support massive connections and increase data rates. We consider a scenario, where a UAV communicates in a downlink underlay cognitive radio based NOMA network (CR-NOMA) with two destination users, a cellular device, and a primary destination following Nakagami- m fading distribution. We study the impact of perfect and imperfect successive interference cancellation (SIC) on outage probability (OP). To help analyze this impact, we derive exact outage results for different network users under perfect and imperfect SIC conditions. Consequently, we make use of Monte Carlo simulations to confirm the analytical results.

This is an open access article under the [CC BY-SA](#) license.



Corresponding Author:

Chi-Bao Le

Faculty of Electronics Technology, Industrial University of Ho Chi Minh City

12 Nguyen Van Bao Road, Go Vap District, Ho Chi Minh City, Vietnam

Email: lechibao@iuh.edu.vn

1. INTRODUCTION

The merging of unmanned aerial vehicles (UAVs) with next generation communications has found significant interest in industry and academia. UAV-assisted communications are expected to provide rapid deployment opportunities, mobility, and reliable line-of-sight (LoS) linkages over traditional ground-based communications [1], [2]. Hence, UAVs will find different roles and applications in future communication networks [3]–[7]. However, UAV-assisted communications face spectrum scarcity issues as they operate in overburdened industrial, scientific, and medical (ISM) bands [1], [8]. To deal with this challenge, underlay cognitive radio (CR) technology has been introduced into UAV-assisted communications to enhance spectrum usage [9]–[14]. In underlay CR networks, so-called secondary users (unlicensed users) can gain access to a primary network by ensuring that interference levels remain constrained below a certain temperature so as not to interfere with the primary network or vice versa.

Despite the many benefits of UAV-CR integration, the UAV battery life is still a major design constraint. Hence, it is important to design UAV-CR networks with transmission efficiency in mind [1]. Non-orthogonal multiple access (NOMA) technology is viewed as a candidate to achieve this goal, owing to its spectrum effectiveness, small latency, and massive connectivity support by simultaneously serving multiple wireless users over the same radio resource via coding at the UAV and successive interference cancellation (SIC) at the user [15]–[27]. Therefore, integrating NOMA with UAV-enabled CR networks shows great promise for future UAV-assisted cellular networks.

Few authors have studied the outage performance of UAV-aided CR networks. For example, in [15]

the authors utilize dynamic spectrum sensing to find empty spectrum. These empty spectra are shared with secondary users, thus, avoiding interfering with primary users. The authors derive outage probability expressions for the proposed system. The majority of work has paid more attention to the outage performance of UAV-enabled NOMA systems [16]–[24]. The works in [16] focused on deriving exact outage results for full-duplex/half-duplex NOMA enabled UAV communications. Specifically, [16] demonstrates the impact of shadowing on full-duplex and half-duplex NOMA. The combination of NOMA and satellite-UAV networks has gained research popularity. The authors consider a network consisting of a satellite serving as a base station to a UAV with decode-forward (DF) functionality communicating with terrestrial users via NOMA technology [17]. The authors assume that the satellite to UAV link follows Rician distribution and UAV-to-users link experiences Nakagami- m distribution. The authors showed that the outage performance is affected by the Nakagami- m channel coefficient. Another area of increasing popularity for UAV application is in underlaid device-to-device (D2D) NOMA-UAV assisted networks as seen in [18]. As well as in internet-of-things (IoT) networks [19]. Finally, there have been several works that have investigated the concept of using UAVs as relays as seen in [20]–[22]. The UAV network relies on NOMA to control interference between ground-based users.

Therefore, in this paper, based on the above ideas, we study the probability of outage of the UAV-assisted underlay CR-NOMA network. Our main contributions are: i) firstly, we derive exact outage expressions of the secondary network users, ii) secondly, from these expressions we analyze the role of successive interference cancellation, interference temperature constraint, and UAV height on outage probability, iii) all expressions are confirmed using Monte Carlo simulations. The paper is organized as follows. In section 2, we describe the proposed system model and channel characteristics. Thereafter, in section 3 we derive closed-form expressions of OP. In section 4, we highlight the results and discussions followed by the summary in section 5.

2. UAV-AIDED UNDERLAY CR-NOMA NETWORK MODEL AND CHANNEL CHARACTERISTICS

2.1. System model

We consider the outage performance of the secondary network (SN) in a downlink underlay CR-NOMA network, as seen in Figure 1. Such SN includes of a secondary source (for example relaying UAV (R)), two destination users (U_1, U_2), other cellular user equipment (CUE) as well as a primary destination (PD). All the channels undergo quasi-static independent but not identically distributed (i.i.n.d) Nakagami- m fading.

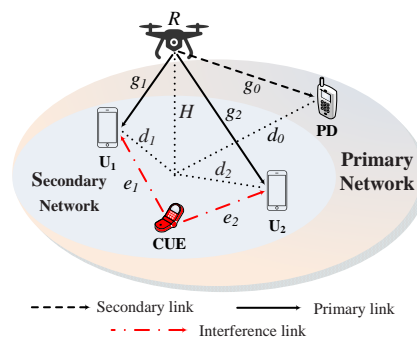


Figure 1. UAV-assisted underlay CR-NOMA network system model

The channel coefficients of the links $R \rightarrow PD$, $R \rightarrow U_1$, $R \rightarrow U_2$, $CUE \rightarrow U_1$, $CUE \rightarrow U_2$ are $g_0 \sim \mathcal{G}\left(m_0, \frac{\lambda_0}{m_0}\right)$, $g_1 \sim \mathcal{G}\left(m_1, \frac{\lambda_{01}}{m_1}\right)$, $g_2 \sim \mathcal{G}\left(m_2, \frac{\lambda_2}{m_2}\right)$, $e_1 \sim \mathcal{CN}(0, \Omega_1)$, $e_2 \sim \mathcal{CN}(0, \Omega_2)$, respectively, with $\mathcal{G}\left(m, \frac{\lambda}{m}\right)$ then follows Gamma distribution with shape m and mean λ and $\mathcal{CN}(x, y)$ the complex normal distribution with average x and variance y . In Figure 1, we can readily represent the locations of two users U_1, U_2 and PD at d_1, d_2 and d_0 , respectively. Based on the above, we can obtain the Euclidean distance from R to U_1 , R to U_2 and R to PD , respectively as:

$$d_{U_1} = \sqrt{d_1^2 + H^2}, d_{U_2} = \sqrt{d_2^2 + H^2}, d_{PD} = \sqrt{d_0^2 + H^2}, \quad (1)$$

where H is the height of UAV. We set channel gains $\lambda_0 = \sqrt{d_{PD}^{-\alpha}}$, $\lambda_1 = \sqrt{d_{U_1}^{-\alpha}}$, $\lambda_2 = \sqrt{d_{U_2}^{-\alpha}}$, $\Omega_{e_1} = \sqrt{d_{e_1}^{-\alpha}}$ and $\Omega_{e_2} = \sqrt{d_{e_2}^{-\alpha}}$ in which α denotes the path loss exponent. In the considered system, the cognitive transmitter intends to send signals to the secondary destinations. To guarantee operation of primary network, the secondary R keeps the transmit power as the following constraint [25], (3).

$$P_R = \min \left(\bar{P}_R, \frac{Q}{|g_0|^2} \right), \tag{2}$$

where \bar{P}_R represents the secondary transmitter maximum power, and Q is the interference temperature constraint (ITC) at the PD . We define \tilde{x}_1 , \tilde{x}_2 and \hat{x}_{CUE} as the signals for U_1 , U_2 and CUE , respectively. In NOMA, power allocation factors are a_1, a_2 , and $a_1 < a_2$, $a_1 + a_2 = 1$. The received signals at the two users are given by [26]:

$$\tilde{y}_{U_i} = g_i \left[\sum_{j=1}^2 \sqrt{a_j P_R} \tilde{x}_j \right] + \sqrt{\kappa P_{CUE}} e_i \hat{x}_{CUE} + \tilde{\omega}_{U_i}, \quad i \in \{1, 2\}, \tag{3}$$

where $\tilde{\omega}_{U_i} \sim \mathcal{CN}(0, N_0)$ is the power of the additive white Gaussian noise (AWGN) equal to N_0 , P_R and P_{CUE} represent the normalized transmission powers at the R and CUE , respectively and κ , $0 \leq \kappa \leq 1$ denotes as scaling factor related to level of interference. From (3), the received signal-to-interference-plus-noise ratio (SINR) can be obtained as:

$$\begin{aligned} \tilde{\gamma}_{U_2 \rightarrow U_1} &= \frac{\rho_R a_2 |g_1|^2}{\rho_R a_1 |g_1|^2 + \kappa \rho_{CUE} |e_1|^2 + 1} \\ &\simeq \frac{\rho_R a_2 |g_1|^2}{\rho_R a_1 |g_1|^2 + \Phi_1}, \end{aligned} \tag{4}$$

where $\rho_R = \frac{P_R}{N_0}$ and $\rho_{CUE} = \frac{P_{RSU}}{N_0}$ are the transmit signal-to-noise ratio (SNR). Note that \tilde{x}_1 , \tilde{x}_2 and \hat{x}_{CUE} are normalized unity power signals, i.e. $\mathbb{E} \{ \tilde{x}_1^2 \} = \mathbb{E} \{ \tilde{x}_2^2 \} = \mathbb{E} \{ \hat{x}_{CUE}^2 \} = 1$ in which $\mathbb{E} [x]$ denotes expectation operation. We assume $\mathbb{E} \{ |e_i|^2 \} = \sqrt{d_{e_i}^{-\alpha}}$, $i \in \{1, 2\}$. Then, we set $\Phi_i = \kappa \rho_{CUE} \sqrt{d_{e_i}^{-\alpha}} + 1$. After SIC, the instantaneous SNR at U_1 for the detection of \tilde{x}_1 is given as:

$$\tilde{\gamma}_{U_1}^{pSIC} \simeq \frac{\rho_R a_1 |g_1|^2}{\Phi_1}, \tag{5}$$

$$\tilde{\gamma}_{U_1}^{ipSIC} \simeq \frac{\rho_R a_1 |g_1|^2}{\rho_R |g_I|^2 + \Phi_1}, \tag{6}$$

where $|g_I|^2 \sim \mathcal{CN}(0, \lambda_I)$ in which $0 \leq \lambda_I < 1$ is the level of residual interference as a result of imperfect SIC in [27]. Given (3), the instantaneous SINR at U_2 to detect \tilde{x}_2 , with \tilde{x}_1 from (3) treated as an interference, thus, from (3), the SINR can be written as:

$$\tilde{\gamma}_{U_2} \simeq \frac{\rho_R a_2 |g_2|^2}{\rho_R a_1 |g_2|^2 + \Phi_1}. \tag{7}$$

2.2. Channel characteristics

The probability density function (PDF) of \bar{X} , $\bar{X} \in g$ is given by [19]:

$$f_{|\bar{X}_i|^2}(x) = \frac{\mu_i^{m_i} x^{m_i-1}}{\Gamma(m_i)} e^{-\mu_i x}, \quad i \in \{0, 1, 2\}, \tag{8}$$

where $\Gamma(x) = (x-1)!$ is the Gamma function and $\mu_i = \frac{m_i}{\lambda_i}$. According to [20] the cumulative distribution functions (CDF) of \bar{X} can be obtained as:

$$F_{|\bar{X}_i|^2}(x) = 1 - e^{-\mu_i x} \sum_{t=0}^{m_i-1} \frac{\mu_i^t x^t}{t!}, \quad i \in \{0, 1, 2\}. \tag{9}$$

Additionally, Rayleigh-distributed random variables (RVs) of $|g_I|^2$ have exponential distributions with $f_{|g_I|^2}(x) = \frac{1}{\lambda_I} e^{-\frac{x}{\lambda_I}}$ and $F_{|g_I|^2}(x) = 1 - e^{-\frac{x}{\lambda_I}}$ in [28].

3. ANALYSIS OF OUTAGE PROBABILITY

Case 1: from (6), the outage probability (OP) of the near user with ipSIC is calculated as:

$$\begin{aligned}
 \mathcal{P}_1^{ipSIC} &= \Pr\left(\tilde{\gamma}_{U_2 \rightarrow U_1} < \varepsilon_2 \mid \tilde{\gamma}_{U_1}^{ipSIC} < \varepsilon_1\right) \\
 &= 1 - \Pr\left(\tilde{\gamma}_{U_2 \rightarrow U_1} \geq \varepsilon_2, \tilde{\gamma}_{U_1}^{ipSIC} \geq \varepsilon_1\right) \\
 &= 1 - \Pr\left(|g_1|^2 \geq \frac{\varepsilon_2 \Phi_1}{\rho_R (a_2 - \varepsilon_2 a_1)}, |g_I|^2 \leq \frac{a_1}{\varepsilon_1} |g_1|^2 - \frac{\Phi_1}{\rho_R}, |g_1|^2 > \frac{\varepsilon_1 \Phi_1}{\rho_R a_1}\right) \\
 &\triangleq 1 - \Pr\left(|g_1|^2 \geq \frac{\phi_{\max}}{\rho_R}, |g_I|^2 \leq \frac{a_1}{\varepsilon_1} |g_1|^2 - \frac{\Phi_1}{\rho_R}\right),
 \end{aligned} \tag{10}$$

where $\varepsilon_j = 2^{2R_j} - 1$, for $j = 1, 2$ is called as target rate at U_j , $\phi_2 = \frac{\varepsilon_2 \Phi_1}{a_2 - \varepsilon_2 a_1}$, $\phi_1 = \frac{\varepsilon_1 \Phi_1}{a_1}$ and $\phi_{\max} = \max(\phi_1, \phi_2)$. Because $P_R = \min\left(\bar{P}_R, \frac{Q}{|g_0|^2}\right)$ in (2) then \mathcal{P}_1^{ipSIC} is given as:

$$\begin{aligned}
 \mathcal{P}_1^{ipSIC} &= 1 - \left[\underbrace{\Pr\left(|g_1|^2 \geq \frac{\phi_{\max}}{\bar{\rho}_R}, |g_I|^2 \leq \frac{a_1}{\varepsilon_1} |g_1|^2 - \frac{\Phi_1}{\bar{\rho}_R}, |g_0|^2 < \frac{\rho_Q}{\bar{\rho}_R}\right)}_{\mathcal{A}_1} \right. \\
 &\quad \left. + \Pr\left(|g_1|^2 \geq \frac{\phi_{\max} |g_0|^2}{\rho_Q}, |g_I|^2 \leq \frac{a_1}{\varepsilon_1} |g_1|^2 - \frac{\Phi_1 |g_0|^2}{\rho_Q}, |g_0|^2 > \frac{\rho_Q}{\bar{\rho}_R}\right) \right]
 \end{aligned} \tag{11}$$

Proposition 1: the exact OP expression at U_1 with ipSIC is given respectively by:

$$\begin{aligned}
 \mathcal{P}_1^{ipSIC} &= 1 - \left\{ \frac{1}{\Gamma(m_0) \Gamma(m_1)} \gamma\left(m_0, \frac{\mu_0 \rho_Q}{\bar{\rho}_R}\right) \left[\Gamma\left(m_1, \frac{\mu_1 \phi_{\max}}{\bar{\rho}_R}\right) - \frac{\mu_1^{m_1}}{\chi_1^{m_1}} e^{-\frac{\Phi_1}{\lambda_I \bar{\rho}_R}} \Gamma\left(m_1, \chi_1 \frac{\phi_{\max}}{\bar{\rho}_R}\right) \right] \right. \\
 &\quad + \frac{\mu_0^{m_0}}{\Gamma(m_0)} \sum_{a=0}^{m_1-1} \frac{\Delta_{\max}^a}{a!} \left[\frac{\mu_1^a}{(\mu_0 + \mu_1 \Delta_{\max})^{m_0+a}} \Gamma\left(m_0 + a, \frac{\rho_Q (\mu_0 + \mu_1 \Delta_{\max})}{\bar{\rho}_R}\right) \right. \\
 &\quad \left. \left. - \frac{\mu_1^{m_1}}{\chi_1^{m_1-a} (\chi_0 + \chi_1 \Delta_{\max})^{m_0+a}} \Gamma\left(m_0 + a, \frac{\rho_Q (\chi_0 + \chi_1 \Delta_{\max})}{\bar{\rho}_R}\right) \right] \right\},
 \end{aligned} \tag{12}$$

where $\gamma(\cdot, \cdot)$ is the lower incomplete Gamma function, $\Gamma(\cdot, \cdot)$ is the upper incomplete Gamma function, $\chi_1 = \mu_1 + \frac{a_1}{\lambda_I \varepsilon_1}$, $\chi_0 = \mu_0 - \frac{\Phi_1}{\lambda_I \rho_Q}$ and $\Delta_{\max} = \max\left(\frac{\phi_{\max}}{\rho_Q}, \frac{\Phi_1 \varepsilon_1}{a_1 \rho_Q}\right)$.

Proof 1: from (11), with the help of (7) and PDF of $|g_I|^2$ we have \mathcal{A}_1 can be further computed by:

$$\begin{aligned}
 \mathcal{A}_1 &= \int_0^{\frac{\rho_Q}{\bar{\rho}_R}} f_{|g_0|^2}(x) \int_{\frac{\phi_{\max}}{\bar{\rho}_R}}^{\infty} f_{|g_1|^2}(y) \int_0^{\frac{a_1 y - \Phi_1}{\varepsilon_1}} f_{|g_I|^2}(z) dx dy dz \\
 &= \frac{\mu_0^{m_0} \mu_1^{m_1}}{\Gamma(m_0) \Gamma(m_1) \lambda_I} \int_0^{\frac{\rho_Q}{\bar{\rho}_R}} e^{-\mu_0 x} x^{m_0-1} \int_{\frac{\phi_{\max}}{\bar{\rho}_R}}^{\infty} e^{-\mu_1 y} y^{m_1-1} \int_0^{\frac{a_1 y - \Phi_1}{\varepsilon_1}} e^{-\frac{z}{\lambda_I}} dx dy dz.
 \end{aligned} \tag{13}$$

Fortunately, the last step can be obtained by using the result reported in [29], (3.351.1) and after some manipulations with the help of [29], (3.351.2) then it can be given as:

$$\begin{aligned}
 \mathcal{A}_1 &= \frac{\mu_1^{m_1}}{\Gamma(m_0)\Gamma(m_1)} \gamma\left(m_0, \frac{\mu_0 \rho_Q}{\bar{\rho}_R}\right) \int_{\frac{\phi_{\max}}{\bar{\rho}_R}}^{\infty} e^{-\mu_1 y} y^{m_1-1} \left(1 - e^{-\frac{1}{\lambda_I} \left(\frac{a_1}{\varepsilon_1} y - \frac{\Phi_1}{\bar{\rho}_R}\right)}\right) dy \\
 &= \frac{\mu_1^{m_1}}{\Gamma(m_0)\Gamma(m_1)} \gamma\left(m_0, \frac{\mu_0 \rho_Q}{\bar{\rho}_R}\right) \left[\int_{\frac{\phi_{\max}}{\bar{\rho}_R}}^{\infty} e^{-\mu_1 y} y^{m_1-1} dy - e^{\frac{\Phi_1}{\lambda_I \bar{\rho}_R}} \int_{\frac{\phi_{\max}}{\bar{\rho}_R}}^{\infty} e^{-(\mu_1 + \frac{a_1}{\lambda_I \varepsilon_1}) y} y^{m_1-1} dy \right] \quad (14) \\
 &= \frac{1}{\Gamma(m_0)\Gamma(m_1)} \gamma\left(m_0, \frac{\mu_0 \rho_Q}{\bar{\rho}_R}\right) \left[\Gamma\left(m_1, \frac{\mu_1 \phi_{\max}}{\bar{\rho}_R}\right) - \frac{\mu_1^{m_1}}{\chi_1^{m_1}} e^{\frac{\Phi_1}{\lambda_I \bar{\rho}_R}} \Gamma\left(m_1, \chi_1 \frac{\phi_{\max}}{\bar{\rho}_R}\right) \right],
 \end{aligned}$$

where $\chi_1 = \mu_1 + \frac{a_1}{\lambda_I \varepsilon_1}$, $\gamma(\cdot, \cdot)$ is the lower incomplete Gamma function and $\Gamma(\cdot, \cdot)$ is the upper incomplete Gamma function. It is further achieved \mathcal{A}_2 as shown in:

$$\begin{aligned}
 \mathcal{A}_2 &= \Pr\left(|g_1|^2 \geq \frac{\phi_{\max} |g_0|^2}{\rho_Q}, |g_I|^2 \leq \frac{a_1}{\varepsilon_1} |g_1|^2 - \frac{\Phi_1 |g_0|^2}{\rho_Q}, |g_0|^2 > \frac{\rho_Q}{\bar{\rho}_R}, |g_1|^2 > \frac{\Phi_1 \varepsilon_1 |g_0|^2}{a_1 \rho_Q}\right) \\
 &= \Pr\left(|g_1|^2 \geq \Delta_{\max} |g_0|^2, |g_I|^2 \leq \frac{a_1}{\varepsilon_1} |g_1|^2 - \frac{\Phi_1 |g_0|^2}{\rho_Q}, |g_0|^2 > \frac{\rho_Q}{\bar{\rho}_R}\right) \\
 &= \int_{\frac{\rho_Q}{\bar{\rho}_R}}^{\infty} f_{|g_0|^2}(x) \int_{\Delta_{\max} x}^{\infty} f_{|g_1|^2}(y) \int_0^{\frac{\frac{a_1}{\varepsilon_1} y - \frac{\Phi_1}{\rho_Q} x}{x}} f_{|g_I|^2}(z) dx dy dz \\
 &= \frac{\mu_0^{m_0} \mu_1^{m_1}}{\Gamma(m_0)\Gamma(m_1)} \int_{\frac{\rho_Q}{\bar{\rho}_R}}^{\infty} e^{-\mu_0 x} x^{m_0-1} \int_{\Delta_{\max} x}^{\infty} e^{-\mu_1 y} y^{m_1-1} \left(1 - e^{-\frac{1}{\lambda_I} \left(\frac{a_1}{\varepsilon_1} y - \frac{\Phi_1}{\rho_Q} x\right)}\right) dx dy \\
 &= \frac{\mu_0^{m_0} \mu_1^{m_1}}{\Gamma(m_0)\Gamma(m_1)} \left[\int_{\frac{\rho_Q}{\bar{\rho}_R}}^{\infty} e^{-\mu_0 x} x^{m_0-1} \int_{\Delta_{\max} x}^{\infty} e^{-\mu_1 y} y^{m_1-1} dx dy - \int_{\frac{\rho_Q}{\bar{\rho}_R}}^{\infty} e^{-\chi_0 x} x^{m_0-1} \int_{\Delta_{\max} x}^{\infty} e^{-\chi_1 y} y^{m_1-1} dx dy \right] \\
 &= \frac{\mu_0^{m_0}}{\Gamma(m_0)} \sum_{a=0}^{m_1-1} \frac{\Delta_{\max}^a}{a!} \left[\frac{\mu_1^a}{(\mu_0 + \mu_1 \Delta_{\max})^{m_0+a}} \Gamma\left(m_0 + a, \frac{\rho_Q (\mu_0 + \mu_1 \Delta_{\max})}{\bar{\rho}_R}\right) \right. \\
 &\quad \left. - \frac{\mu_1^{m_1}}{\chi_1^{m_1-a} (\chi_0 + \chi_1 \Delta_{\max})^{m_0+a}} \Gamma\left(m_0 + a, \frac{\rho_Q (\chi_0 + \chi_1 \Delta_{\max})}{\bar{\rho}_R}\right) \right], \quad (15)
 \end{aligned}$$

where $\chi_0 = \mu_0 - \frac{\Phi_1}{\lambda_I \rho_Q}$ and $\Delta_{\max} = \max\left(\frac{\phi_{\max}}{\rho_Q}, \frac{\Phi_1 \varepsilon_1}{a_1 \rho_Q}\right)$. Combining (18) and (17) into (10), we can obtain (11). The proof 1 is completed.

Case 2: from (5), the OP of U_1 with pSIC is calculated as:

$$\begin{aligned}
 \mathcal{P}_1^{pSIC} &= 1 - \Pr\left(\tilde{\gamma}_{U_2 \rightarrow U_1} \geq \varepsilon_2, \tilde{\gamma}_{U_1}^{pSIC} \geq \varepsilon_1\right) \\
 &= 1 - \Pr\left(|g_1|^2 \geq \frac{\phi_{\max}}{\rho_R}\right) \\
 &= 1 - \left[\underbrace{\Pr\left(|g_1|^2 \geq \frac{\phi_{\max}}{\bar{\rho}_R}, |g_0|^2 < \frac{\rho_Q}{\bar{\rho}_R}\right)}_{\mathcal{B}_1} + \underbrace{\Pr\left(|g_1|^2 \geq \frac{\phi_{\max}}{\rho_Q} |g_0|^2, |g_0|^2 > \frac{\rho_Q}{\bar{\rho}_R}\right)}_{\mathcal{B}_2} \right]. \quad (16)
 \end{aligned}$$

Proposition 2: the OP at the U_1 with pSIC is given given by:

$$\mathcal{P}_1^{pSIC} = 1 - \sum_{a=0}^{m_1-1} \frac{\mu_1^a \phi_{\max}^a}{a! \Gamma(m_0)} \left[\frac{e^{-\frac{\mu_1 \phi_{\max}}{\bar{\rho}_R}}}{\bar{\rho}_R^a} \gamma \left(m_0, \frac{\mu_0 \rho_Q}{\bar{\rho}_R} \right) + \frac{\rho_Q^{m_0} \mu_0^{m_0}}{(\rho_Q \mu_0 + \mu_1 \phi_{\max})^{m_0+a}} \Gamma \left(m_0 + a, \frac{\rho_Q}{\bar{\rho}_R} \left(\mu_0 + \frac{\mu_1 \phi_{\max}}{\rho_Q} \right) \right) \right]. \quad (17)$$

Proof 2: in (16), we have \mathcal{B}_1 and \mathcal{B}_2 are calculated by:

$$\begin{aligned} \mathcal{B}_1 &= \int_0^{\frac{\rho_Q}{\bar{\rho}_R}} f_{|g_0|^2}(x) \int_{\frac{\phi_{\max}}{\bar{\rho}_R}}^{\infty} f_{|g_1|^2}(y) dx dy \\ &= \frac{\mu_0^{m_0}}{\Gamma(m_0)} \int_0^{\frac{\rho_Q}{\bar{\rho}_R}} x^{m_0-1} e^{-\mu_0 x} \left[1 - F_{|g_1|^2} \left(\frac{\phi_{\max}}{\bar{\rho}_R} x \right) \right] dx, \end{aligned} \quad (18)$$

and

$$\begin{aligned} \mathcal{B}_2 &= \int_{\frac{\rho_Q}{\bar{\rho}_R}}^{\infty} f_{|g_0|^2}(x) \left[1 - F_{|g_1|^2} \left(\frac{\phi_{\max}}{\rho_Q} x \right) \right] dx \\ &= \sum_{a=0}^{m_1-1} \frac{\mu_1^a \phi_{\max}^a \mu_0^{m_0}}{a! \rho_Q^a \Gamma(m_0)} \int_{\frac{\rho_Q}{\bar{\rho}_R}}^{\infty} x^{m_0+a-1} e^{-(\mu_0 + \frac{\mu_1 \phi_{\max}}{\rho_Q}) x} dx. \end{aligned} \quad (19)$$

Respectively. It is noted that the last step can be achieved by using [29], (3.351.1) for \mathcal{B}_1 and [29], (3.351.2) for \mathcal{B}_2 , we have:

$$\mathcal{B}_1 = \sum_{a=0}^{m_1-1} \frac{\mu_1^a \phi_{\max}^a e^{-\frac{\mu_1 \phi_{\max}}{\bar{\rho}_R}}}{a! \bar{\rho}_R^a \Gamma(m_0)} \gamma \left(m_0, \frac{\mu_0 \rho_Q}{\bar{\rho}_R} \right), \quad (20)$$

$$\mathcal{B}_2 = \sum_{a=0}^{m_1-1} \frac{\mu_1^a \phi_{\max}^a \rho_Q^{m_0} \mu_0^{m_0}}{a! \Gamma(m_0) (\rho_Q \mu_0 + \mu_1 \phi_{\max})^{m_0+a}} \Gamma \left(m_0 + a, \frac{\rho_Q}{\bar{\rho}_R} \left(\mu_0 + \frac{\mu_1 \phi_{\max}}{\rho_Q} \right) \right). \quad (21)$$

Substituting (20) and (21) into (12), we can result (13). The proof 2 is completed. Finally, the OP of \mathcal{P}_2 is given by:

$$\begin{aligned} \mathcal{P}_2 &= 1 - \Pr \left(|g_2|^2 \geq \frac{\bar{\phi}_2}{\rho_R} \right) \\ &= 1 - \left[\Pr \left(|g_2|^2 \geq \frac{\bar{\phi}_2}{\bar{\rho}_R}, |g_0|^2 < \frac{\rho_Q}{\bar{\rho}_R} \right) + \Pr \left(|g_2|^2 \geq \frac{\bar{\phi}_2}{\rho_Q} |g_0|^2, |g_0|^2 > \frac{\rho_Q}{\bar{\rho}_R} \right) \right]. \end{aligned} \quad (22)$$

Similarly, by solving \mathcal{P}_1^{pSIC} in (17), \mathcal{P}_2 can be obtained as:

$$\begin{aligned} \mathcal{P}_2 &= 1 - \sum_{b=0}^{m_2-1} \frac{\mu_2^b \bar{\phi}_2^b}{b! \Gamma(m_0)} \left[\frac{e^{-\frac{\mu_2 \bar{\phi}_2}{\bar{\rho}_R}}}{\bar{\rho}_R^b} \gamma \left(m_0, \frac{\mu_0 \rho_Q}{\bar{\rho}_R} \right) + \frac{\rho_Q^{m_0} \mu_0^{m_0}}{(\rho_Q \mu_0 + \mu_2 \bar{\phi}_2)^{m_0+b}} \Gamma \left(m_0 + b, \frac{\rho_Q}{\bar{\rho}_R} \left(\mu_0 + \frac{\mu_2 \bar{\phi}_2}{\rho_Q} \right) \right) \right], \end{aligned} \quad (23)$$

where $\bar{\phi}_2 = \frac{\varepsilon_2 \Phi_2}{a_2 - \varepsilon_2 a_1}$.

4. NUMERICAL RESULTS

We set $m_0 = m_1 = m_2 = m = 2$, $\rho_Q = 25$ (dB), $\rho_{CUE} = 40$ (dB), $\kappa = 0.001$, $\lambda_I = 0.001$, the height of UAV $H = 45$ m, Suppose that $d_0 = 10$ m, $d_1 = 15$ m, $d_2 = 40$ m, $d_{e_1} = 15$ m, $d_{e_2} = 10$ m and the path-loss factor as $\alpha = 2$, the target rates $R_1 = 1$ bps/Hz, $R_2 = 0.5$ bps/Hz, the power allocation coefficients $a_1 = 0.2$ and $a_2 = 0.8$. Monte-Carlo results averaging over 10^7 independent channel realizations. Figure 2 plots OP and UAV transmit SNR relationship, with $m = 1$ and $m = 2$. In (11), (13) and (15) are used to plot the analytical lines. From Figure 2, we notice that the primary network users experience different outage performances depending on the Nakagami- m fading conditions and whether or not SIC is used. We also observe that the performance curves approach an OP floor at 45 dB. We can see the analytical curves fit with Monte Carlo simulations.

Figure 3 plots the OP relationship between outage and UAV transmit SNR, with or without ITC. From Figure 3, we notice that the outage performance curves of P_2 and P_1^{ipSIC} do not approach a floor when ITC is not used. This highlights the impact of SIC and ITC on OP.

Figure 4 plots the relationship between OP and PD transmit SNR, with $m = 3$ and $\bar{\rho}_R = 30$ dB. From Figure 4, we observe that the primary network users experience different outage performances depending on the conditions of SIC. We also observe that the performance curves approach an outage probability floor at 18 dB. Figure 5 plots the relationship between OP and UAV height, with $\bar{\rho}_R = 40$ dB. From Figure 5, we observe that UAV height has significant impact on OP. OP decreases when the UAV moves further away from the users until it approaches a ceiling.

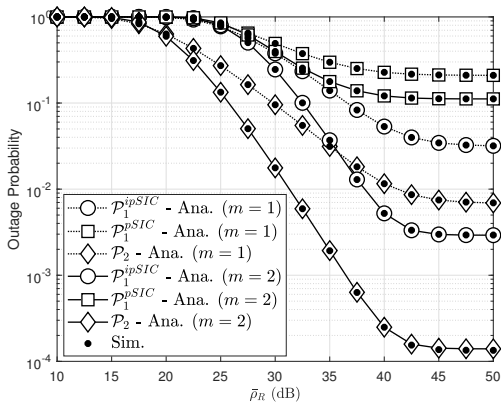


Figure 2. Outage probability versus $\bar{\rho}_R$ in dB with varying $m = 1$ and $m = 2$

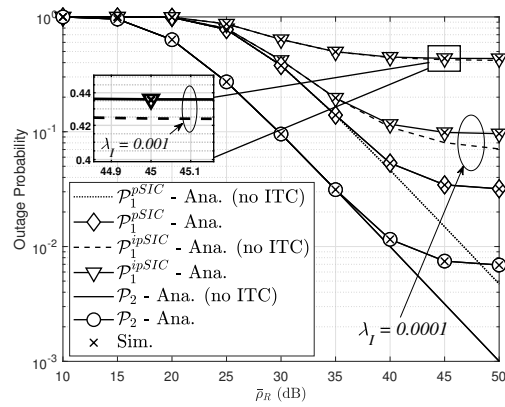


Figure 3. Outage probability versus $\bar{\rho}_R$ in dB with varying ITC with $m = 2$

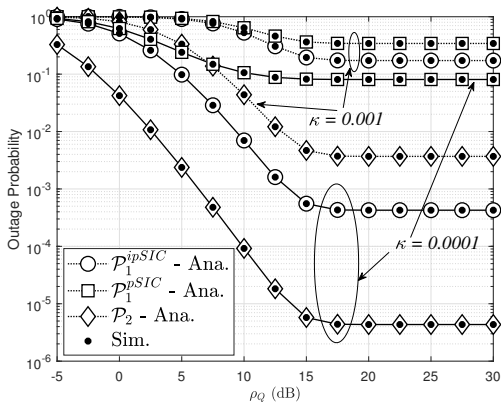


Figure 4. Outage probability versus ρ_Q in dB with $m = 3$ and $\bar{\rho}_R = 30$ (dB)

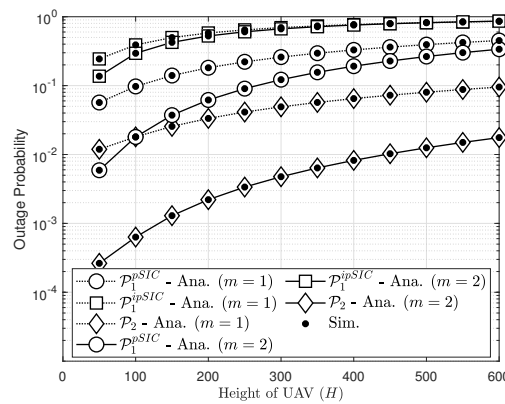


Figure 5. Outage probability versus H with varying $m = 1$ and $m = 2$ and $\bar{\rho}_R = 40$ (dB)

5. CONCLUSION

In this paper, we provided the OP analysis of an underlay CR assisted NOMA-UAV network. We derived exact solutions of OP for different primary network users. We observe from the simulation results, that the height of the UAV, ITC, and hardware capabilities for SIC at the users contributes to the OP of the network. In future work, we will consider ergodic capacity of the system.





REFERENCES

- [1] N. Tang, H. Tang, B. Li, and X. Yuan, "Cognitive NOMA for UAV-Enabled Secure Communications: Joint 3D Trajectory Design and Power Allocation," in *IEEE Access*, vol. 8, pp. 159965–159978, 2020, doi: 10.1109/ACCESS.2020.3020821.
- [2] W. Shi, H. Zhou, J. Li, W. Xu, N. Zhang, and X. Shen, "Drone Assisted Vehicular Networks: Architecture, Challenges and Opportunities," in *IEEE Network*, vol. 32, no. 3, pp. 130–137, May/Jun. 2018, doi: 10.1109/MNET.2017.1700206.
- [3] M. Mozaffari, W. Saad, M. Bennis, Y. -H. Nam and M. Debbah, "A Tutorial on UAVs for Wireless Networks: Applications, Challenges, and Open Problems," in *IEEE Communications Surveys & Tutorials*, vol. 21, no. 3, pp. 2334–2360, 2019, doi: 10.1109/COMST.2019.2902862.
- [4] Y. Zeng, R. Zhang, and T. J. Lim, "Wireless communications with unmanned aerial vehicles: opportunities and challenges," in *IEEE Communications Magazine*, vol. 54, no. 5, pp. 36–42, May 2016, doi: 10.1109/MCOM.2016.7470933.
- [5] I. Bor-Yaliniz, M. Salem, G. Senerath, and H. Yanikomeroglu, "Is 5G Ready for Drones: A Look into Contemporary and Prospective Wireless Networks from a Standardization Perspective," in *IEEE Wireless Communications*, vol. 26, no. 1, pp. 18–27, Feb. 2019, doi: 10.1109/MWC.2018.1800229.
- [6] A. Fotouhi *et al.*, "Survey on UAV Cellular Communications: Practical Aspects, Standardization Advancements, Regulation, and Security Challenges," in *IEEE Communications Surveys & Tutorials*, vol. 21, no. 4, pp. 3417–3442, 2019, doi: 10.1109/COMST.2019.2906228.
- [7] Y. Zeng, Q. Wu, and R. Zhang, "Accessing From the Sky: A Tutorial on UAV Communications for 5G and Beyond," in *Proceedings of the IEEE*, vol. 107, no. 12, pp. 2327–2375, Dec. 2019, doi: 10.1109/JPROC.2019.2952892.
- [8] S. R. Sabuj, A. Ahmed, Y. Cho, K. -J. Lee and H. -S. Jo, "Cognitive UAV-Aided URLLC and mMTC Services: Analyzing Energy Efficiency and Latency," in *IEEE Access*, vol. 9, pp. 5011–5027, 2021, doi: 10.1109/ACCESS.2020.3048436.
- [9] W. Mei and R. Zhang, "UAV-Sensing-Assisted Cellular Interference Coordination: A Cognitive Radio Approach," in *IEEE Wireless Communications Letters*, vol. 9, no. 6, pp. 799–803, Jun. 2020, doi: 10.1109/LWC.2020.2970416.
- [10] K. B. Letaief and W. Zhang, "Cooperative Communications for Cognitive Radio Networks," in *Proceedings of the IEEE*, vol. 97, no. 5, pp. 878–893, May 2009, doi: 10.1109/JPROC.2009.2015716.
- [11] T. Yucek and H. Arslan, "A Survey of Spectrum Sensing Algorithms for Cognitive Radio Applications," in *IEEE Communications Surveys & Tutorials*, vol. 11, no. 1, pp. 116–130, 2009, doi: 10.1109/SURV.2009.090109.
- [12] Y. Liang, K. Chen, G. Y. Li, and P. Mahonen, "Cognitive Radio Networking and Communications: An Overview," in *IEEE Transactions on Vehicular Technology*, vol. 60, no. 7, pp. 3386–3407, Sep. 2011, doi: 10.1109/TVT.2011.2158673.
- [13] G. Ganesan and Y. Li, "Cooperative Spectrum Sensing in Cognitive Radio, Part I: Two User Networks," in *IEEE Transactions on Wireless Communications*, vol. 6, no. 6, pp. 2204–2213, Jun. 2007, doi: 10.1109/TWC.2007.05775.
- [14] G. Ganesan and Ye Li, "Cooperative Spectrum Sensing in Cognitive Radio Networks," *First IEEE International Symposium on New Frontiers in Dynamic Spectrum Access Networks, 2005. DySPAN 2005.*, 2005, pp. 137–143, doi: 10.1109/DYSPAN.2005.1542628.
- [15] B. Tıgılı, E. Erdem, and E. Erdoğan, "Outage Probability Performance of Cognitive Radio Enabled UAV Relaying," *2020 28th Signal Processing and Communications Applications Conference (SIU)*, Gaziantep, Turkey, 2020, pp. 1–4. doi: 10.1109/SIU49456.2020.9302131.
- [16] H. E. T. Zheng, A. S. Madhukumar, R. P. Sirigina, and A. K. Krishna, "An Outage Probability Analysis of Full-Duplex NOMA in UAV Communications," *2019 IEEE Wireless Communications and Networking Conference (WCNC)*, 2019, pp. 1–5. doi: 10.1109/WCNC.2019.8886161.
- [17] C. Wang, X. Yang, Q. Du, and J. Wang, "Outage Performance of Satellite-UAV Network Framework based on NOMA," *2021 IEEE 5th International Conference on Cryptography, Security and Privacy (CSP)*, 2021, pp. 171–175, doi: 10.1109/CSP51677.2021.9357597.
- [18] M. M. Selim, M. Rihan, Y. Yang, L. Huang, Z. Quan, and J. Ma, "On the Outage Probability and Power Control of D2D Underlying NOMA UAV-Assisted Networks," in *IEEE Access*, vol. 7, pp. 16525–16536, 2019, doi: 10.1109/ACCESS.2019.2894390.
- [19] T. Shen and H. Ochiai, "A UAV-Enabled Wireless Powered Sensor Network Based on NOMA and Cooperative Relaying With Altitude Optimization," in *IEEE Open Journal of the Communications Society*, vol. 2, pp. 21–34, 2021. doi: 10.1109/OJCOMS.2020.3042257.
- [20] L. Wang, B. Hu, S. Chen, and J. Cui, "UAV-Enabled Reliable Mobile Relaying Based on Downlink NOMA," in *IEEE Access*, vol. 8, pp. 25237–25248, 2020, doi: 10.1109/ACCESS.2020.2970206.
- [21] T. Z. H. Ernest, A. S. Madhukumar, R. P. Sirigina, and A. K. Krishna, "NOMA-Aided UAV Communications over Correlated Rician Shadowed Fading Channels," in *IEEE Transactions on Signal Processing*, vol. 68, pp. 3103–3116, 2020, doi: 10.1109/TSP.2020.2994781.
- [22] P. K. Sharma and D. I. Kim, "UAV-Enabled Downlink Wireless System with Non-Orthogonal Multiple Access," *2017 IEEE Globecom Workshops (GC Wkshps)*, 2017, pp. 1–6. doi: 10.1109/GLOCOMW.2017.8269066.
- [23] M. Monemi, H. Tabassum, and R. Zahedi, "On the Performance of Non-Orthogonal Multiple Access (NOMA): Terrestrial vs. Aerial Networks," *2020 IEEE Eighth International Conference on Communications and Networking (ComNet)*, 2020, pp. 1–8. doi: 10.1109/ComNet47917.2020.9306102.
- [24] S. K. Zaidi, S. F. Hasan, and X. Gui, "Outage Analysis of Ground-Aerial NOMA With Distinct Instantaneous Channel Gain Ranking," in *IEEE Transactions on Vehicular Technology*, vol. 68, no. 11, pp. 10775–10790, Nov. 2019. doi: 10.1109/TVT.2019.2938516.
- [25] Dinh-Thuan Do, Anh-Tu Le, and B. M. Lee, "NOMA in Cooperative Underlay Cognitive Radio Networks Under Imperfect SIC,"





- in *IEEE Access*, vol. 8, pp. 86180–86195, 2020, doi: 10.1109/ACCESS.2020.2992660.
- [26] Chi-Bao Le, Dinh-Thuan Do, Z. D. Zaharis, C. X. Mavromoustakis, G. Mastorakis, and E. K. Markakis, "System Performance Analysis in Cognitive Radio-Aided NOMA Network: An Application to Vehicle-to-Everything Communications," *Wireless Personal Communications*, vol. 120, no. 3, pp. 1975–2000, Feb. 2021, doi: 10.1007/s11277-021-08273-x.
- [27] Thi-Anh Hoang, Chi-Bao Le, and Dinh-Thuan Do, "OSecurity performance analysis for power domain NOMA employing in cognitive radio networks," *Bulletin of Electrical Engineering and Informatics*, vol. 9, no. 3, pp. 1046–1054, Jun. 2020, doi: 10.11591/eei.v9i3.163.
- [28] D. -T. Do, C. -B. Le, and F. Afghah, "Enabling full-duplex and energy harvesting in uplink and downlink of small-cell network relying on power domain based multiple access," in *IEEE Access*, vol. 8, pp. 142772–142784, 2020, doi: 10.1109/ACCESS.2020.3013912.
- [29] I. S. Gradshteyn and I. M. Ryzhik, *Table of Integrals, Series and Products*, 2000.

BIOGRAPHIES OF AUTHORS



Dinh-Thuan Do     (Senior Member, IEEE) received the B.S., M.Eng., and Ph.D. degrees in communications engineering from Vietnam National University (VNU-HCM), in 2003, 2007, and 2013, respectively. His research interests include signal processing in wireless communications networks, cooperative communications, non-orthogonal multiple access, full-duplex transmission, and energy harvesting. He can be contacted at email: dodinhthuan@iuh.edu.vn and dodinhthuan@gmail.com.



Chi-Bao Le     was born in Binh Thuan, Vietnam. He has worked closely with Dr. Thuan at the Wireless Communications and Signal Processing Research Group, Industrial University of Ho Chi Minh City, Vietnam. His research interests include electronic design, signal processing in wireless communications networks, non-orthogonal multiple access, and physical layer security. He can be contacted at email: lechibao@iuh.edu.vn.